Proceedings of the
Annual Stability Conference
Structural Stability Research Council
Atlanta, Georgia, April 21-24, 2026

Distributed measurement of thermal behavior in metal roof panels under high diurnal temperature conditions

Malik Umer Farooq[1], Hyeyoung Koh[2]

Abstract

High heat events such as heatwaves amplify diurnal temperature variations compared to typical hot days, resulting in more rapid and repeated heating-cooling cycles. These cycles induce recurrent thermal movement in structural components, contributing to cumulative deformation and raising long-term stability concerns. Large diurnal swings also lead to nonuniform temperature fields, which complicate design and performance assessment. However, current steel design practices often overlook the transient and cyclic nature of diurnal thermal effects, even as structures are increasingly exposed to extreme heat. It is therefore important to understand how these temperature fields evolve and interact with structural responses during such events.

This study investigated the thermal fatigue response of metal roof systems under real-world heat conditions in Eastern Washington, where extreme heat events are becoming more frequent and intense. Corrugated metal roof decks, commonly subjected to thermal expansion and contraction, were installed outdoors to capture natural diurnal heat loading. Distributed fiber optic sensors for temperature and strain were installed along 12-ft simply supported span decks to record time- and space-varying thermal stresses. The resulting experimental data were used to develop nonuniform temperature fields that characterize the magnitude and temporal evolution of thermal cycles. The major findings of this experimental work demonstrated that the temperature and corresponding stress fields are nonuniform, and that strain gradients exist between the top surface (exposed to sunlight) and the bottom surface (shaded from sunlight). These results enhance understanding of the influence of thermally induced stress distributions in steel component behavior. The findings suggest that thermal effects may merit consideration in design and could be related to long-term stability risks for steel structures subjected to thermal demands.

1 Introduction

Metal roofs are widely used in industrial warehouses and in sports arenas, because of their high strength-to-weight ratio and suitability for long spans (Wang et al., 2022). In the United States, nearly 65% of newly constructed low-rise buildings which require long span such as industrial

[1]Graduate Research Assistant, Washington State University, Pullman, WA, <malik.farooq@wsu.edu>
[2]Assistant Professor, Washington State University, Pullman, WA, <hyeyoung.koh@wsu.edu>

complexes, sports stadiums and aircraft hangers use metal roofing systems (Dabral and Ewing, n.d.). These systems typically employ thin-gauge steel panels that are directly exposed to solar radiation, which make them highly susceptible to substantial temperature fluctuations. Prolonged solar exposure produces uneven temperature fields (Wang et al., 2025). This leads to repetitive expansion and contraction cycles. Over time, these thermal cycles can weaken stability and reduce material durability (Xu et al., 2020). Because roof systems are essential in building safety, durability, and resilience, particularly under intensifying, their thermal performance requires detailed study (Liu et al., 2025). A growing volume of research highlights the significant thermal effects experienced by metal roofs during extreme heat events. Many studies have focused on assessing the effect of on roof metals. For example, in continuously welded stainless steel roof, a 1°C temperature increase can raise maximum stress by 2.25 MPa and displacement by 0.02 mm, respectively (Chong et al., 2025). Long-term exposure to the sun, excellent thermal conductivity of steel and its direct exposure to the sun, temperature fields vary markedly across roof surfaces (Zhou et al., 2020). Such variations become most pronounced during the afternoon peak, when temperature differences can exceed 20°C under various weather conditions (Wang et al., 2023a). Even small temperature gradients can induce nonuniform stress distributions that result in microcrack formation in large-span steel structures (Xu et al., 2020).

Despite these observations, traditional steel testing often assumes steady-state temperature conditions, which neglects transient and cyclic thermal loads experienced during high temperatures. (Viljoen and Hugo, 2024). Recent experimental work has shown that stainless steel roof panels can experience temperature differences of over 34.3°C relative to ambient temperature, with inclination angle significantly affecting temperature distribution (Wang et al., 2023b). However, most existing studies focus on stainless steel or continuously welded stainless steel roof systems. In contrast, the behavior of purlin bearing rib (PBR) panels, widely used in metal roofing due to their strong interpanel lapping and enhanced structural performance, remains insufficiently explored under high temperatures. To address this gap, this paper presents an assessment of time-varying and nonuniform temperature field of PBR roof panels subjected to high temperatures. An experimental investigation was conducted using distributed fiber optic sensing (DFOS) to monitor temperature and strain along the full length of a PBR panel exposed to solar radiation. Unlike traditional sensors that provide discrete measurements, DFOS offers distributed data, enabling detailed evaluation of temperature field evolution along the fiber. Measurements were collected under three solar exposure scenarios to characterize diurnal thermal behavior across the panel's clear span. The results provide new insights into the temperature field development in PBR roofs and contribute to understanding the growing impacts of high temperatures on steel roofing systems.

2 Test Setup

2.1 Test Specimen

A purlin bearing ribs (PBR) panel was tested in this study. PBR panels incorporate a ribbed design with a purlin bearing leg that increases roof strength by providing full bearing at the panel overlaps. This configuration improves load-bearing capacity and offeres advantages in installation efficiency. PBR panels are fastened directly to purlins, similar to ribbed (R) panels; however, the extended leg provides additional support to the overlapping ribs, which makes them more advantageous than R panels. Other profiles, such as standing seam panels, are installed using floating systems (e.g.,

two-piece or sliding clips), which require more complex installation and therefore increase overall cost. The simplicity of PBR panel construction makes them cost-effective for large-scale projects. Fig. 1 illustrates the cross-section of the specimen, where the ribs are spaced 12 inches apart and rise $\frac{1}{4}$ inches.

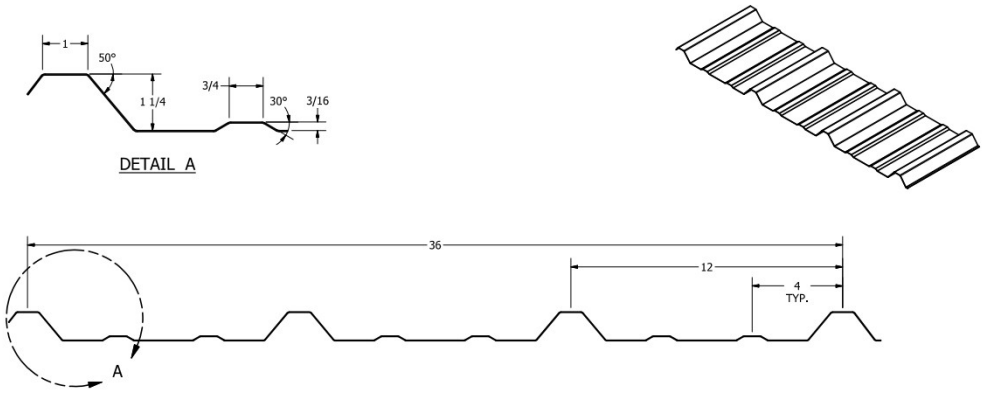

Figure 1: PBR panel profile (Courtesy of ASC building production)

2.2 Distributed Fiber Optic Sensing

Distributed fiber optic sensing (DFOS) offers significant advantages over traditional sensors due to their ability to provide distributed measurements throughout the fiber length (Roman et al., 2020). Additionally, their capability to provide continuous, distributed measurements has significantly contributed to their growing adoption in monitoring the health and integrity of civil infrastructure (Yang et al., 2019). DFOS systems utilizes inhomogeneities within the fiber optic cables to measure small changes along the length of the fiber to capture induced strains (Lu et al., 2019). The fiber optic sensing method used to analyze strain and temperature in the steel deck is Rayleigh OFDR. Rayleigh OFDR uses a swept-frequency laser pulse to generate an interference pattern from the back scattered light which is analyzed to return location and strain information along a fiber optic cable (Ma et al., 2022). Distributed temperature measurements obtained from DFOS are based on Rayleigh scattering in a single-mode optical fiber. Rayleigh scattering originates when light interacts with inhomogeneities in a continuum of matter, dimensions of continuum of matter are smaller than the wavelength of light. Change in temperature induce variations in both the refractive index and the physical length of the optical fiber, resulting in measurable shifts in the Rayleigh back scattered spectra. Change in temperature is determined by using spectral shift technique (Roman et al., 2020). The ODiSI 7100 Rayleigh OFDR system manufactured by LUNA Innovations was used to measure temperature and strain simultaneously. Fiber sensors were installed along the clear span of the roof to provide the continuous measurements. Gauge length of system was 1.3 mm with a sampling rate of 6.25 Hz. In this system, the gauge length is defined as the smallest spatial interval over which strain or temperature values are measured.

2.3 Instrumentation

A 22-gauge PBR panel (3 ft by 16 ft) was used for the experimental work and was fastened to lumber using screws to ensure stability, as illustrated in Fig. 2a. A clear span of 12 ft was used to evaluate the effect of varying temperature on the roof panel. The blue and red lines represent the strain and temperature sensors, respectively, as shown in Fig. 2b.

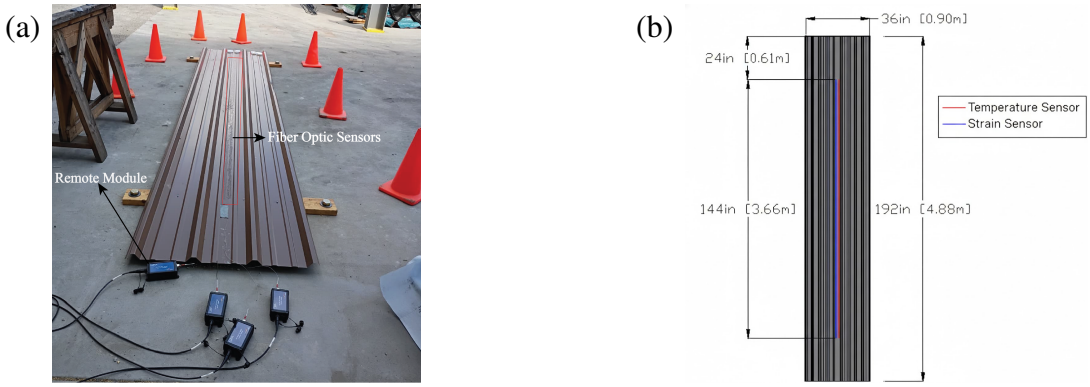

Figure 2: Instrumentation and panel details: (a) Test setup; (b) deck configurations, including fiber optic cable layout diagram.

Fig. 3 shows the installation of sensors on the roof panel. Prior to installing the fiber optic sensor, the roof panel surface was cleaned with acetone. The sensors were bonded to the roof panel using adhesive, and a continuous layer of silicone was applied along the sensor length to protect them. Strain sensors were installed on both the top and bottom surfaces of the roof panel, while a temperature sensor was installed on the top surface to monitor temperature variation along the clear span. The sensors were connected to a remote module, which was then connected to the interrogator for data acquisition. Strain and temperature measurements were collected from the corresponding sensors throughout the test.

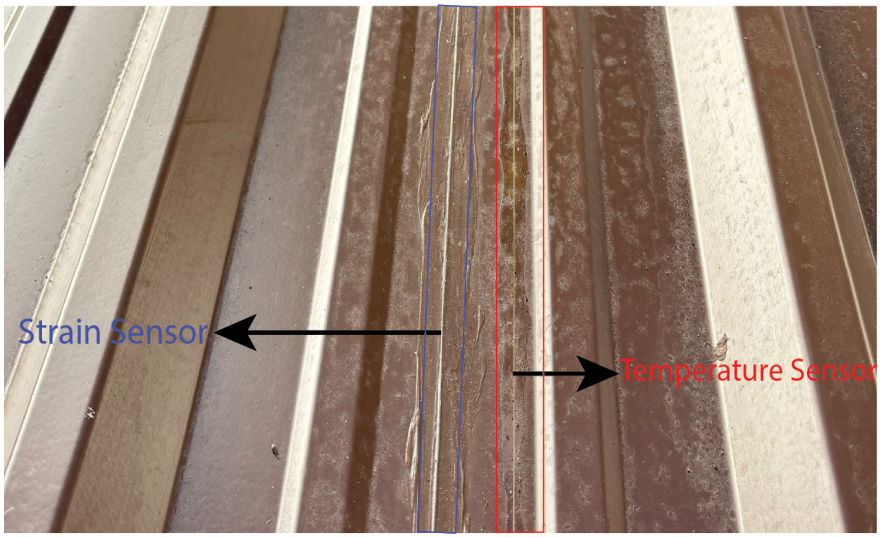

Figure 3: Sensor layout for roof panel

2.4 Testing Procedure

The experiment was performed in Pullman, Washington State, on August 12th over a four-hour period. Tests were conducted at one-hour intervals to obtain corresponding temperature and strain values. Strain and temperature values were collected by assuming different scenarios, depending on the panel's exposure to the sunlight. Following scenarios were considered to collect the data:

- When roof panel is fully exposed to sun light.
- When roof panel started getting shadow due to surrounding buildings.
- When roof panel is under full shadow due to the surrounding buildings.

3 Results

This section presents the outcomes of the study that focused on investigating the thermal behavior of metal roof panel under high temperatures. Three different scenarios were considered to evaluate thermal behavior under varying temperature conditions. All data were obtained from fiber optic sensors, and the analysis was conducted using Python scripts. Distinct thermal responses of the roof panels were observed under different exposure conditions and are summarized using graphical representations.

3.1 Temperature

A comparison was performed between publicly available ambient temperature data for August 12, 2025, in Pullman, Washington state, and the roof surface temperatures measured by the sensors. Fig. 4 shows a significant difference between the two temperature profiles. When the roof was exposed to direct sunlight, the roof temperature was 10°C higher than the ambient temperature. When the roof became shaded, this difference decreased to about 5 °C. However, when the roof panel was fully shaded, the difference between ambient and roof temperature increased to 20 °C. These observations raise important implications for structural design practice, as design is typically based on ambient temperature (Chong et al., 2025), which in this experiment was substantially lower than the actual roof temperature.

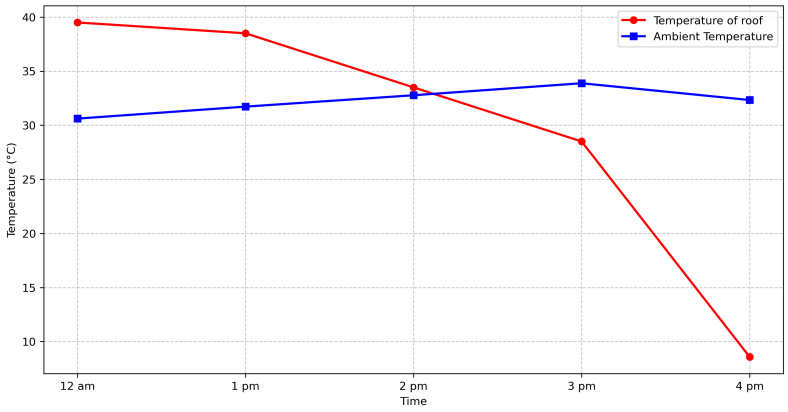

Figure 4: Comparison of ambient temperature with the temperature measured at the roof panel surface

As shown in Fig. 5, exposure of direct sunlight is a dominant factor influencing the temperature field along the metal roof. Full solar exposure produces the highest temperature profile across the entire gauge length. Temperatures generally ranged between 32 °C and 35 °C, with an initial peak reaching 38.5 °C. The anomalous peak, in which the temperature suddenly raised to nearly 38.5 °C before stabilizing, indicates the presence of an external influence beyond typical direct sunlight. This localized heating is attributed to reflection from a nearby glass building facade, which concentrated additional solar energy onto a specific section of the roof panel. In contrast, the remaining portion of the profile indicates consistent heating due to uniform direct solar radiation along the roof span.

The partially exposed condition is represented by the green curve in Fig. 5. A transition zone is observed where the roof shifts from shaded conditions to full sunlight. The temperature remains relatively low, staying 14.8 °C, up to the 1.5-m location. Beyond this point, a sharp increase in temperature occurs with a rise of 22.5 °C within a span of 0.25-m. After 1.75 meter mark, the temperature stabilizes within a range of 32 °C to 34 °C, corresponding to full solar exposure.

The blue line in Fig. 5 represents the core temperature of the roof when fully shaded. Under this condition, the temperature remained uniformly low and stable throughout the length of the temperature sensor. Values ranged from 5 °C to 8 °C, with very little fluctuation compared to the roof panel fully and partiality exposed to the sunlight. There is a difference of 25.5 °C to 28 °C when compared with the temperature values obtained from the roof panel under full sunlight exposure.

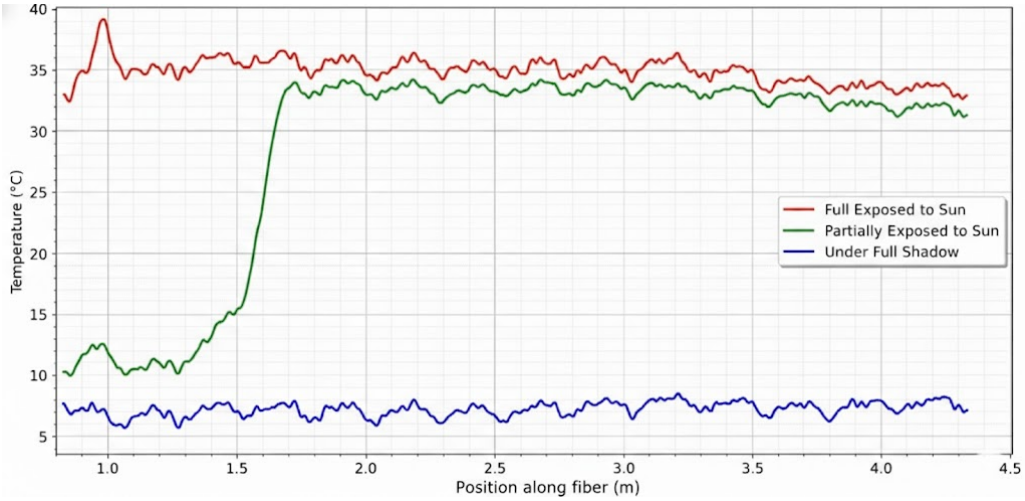

Figure 5: Temperature variations of the panel under all scenarios

3.2 Strain

Strain sensors were installed at both the top and bottom surfaces of the metal roof panel to measure strain corresponding to temperature changes. A comparative graph was prepared to summarize how variations in temperature influence the strain response of the metal roof panel under different exposure conditions.

3.2.1 Bottom Strain

Bottom strain values were analyzed for exposure scenarios to evaluate the relationship between temperature change and strain response. The red curve in Fig. 6 represents the strain distribution when the roof is fully exposed to direct sunlight. Under this condition, the entire steel roof panel is uniformly heated, resulting in thermal expansion along its full length. The sensor recorded consistently high strain values, ranging between 700 to 950 $\mu\epsilon$.

Strain values for the partially exposed condition are represented by the green curve in Fig. 6. In the shaded section, between 0.8 m to 1.4 m, the strain remains low at 300.8 $\mu\epsilon$. This is followed by a sharp and nearly vertical increase of 600.5 $\mu\epsilon$ between 1.4 m and 1.6 m as the roof transitions from shadow into direct sunlight. This behavior indicates localized thermal expansion and the development of a concentrated tensile strain zone at the boundary between shaded and sunlight regions. Beyond this transition zone, the strain fluctuates within a range of 700 to 850 $\mu\epsilon$ under full solar exposure.

The blue curve in Figure. 6 represents the fully shaded condition. Under this scenario, the roof panel exhibits relatively stable behavior along its length. The measured strain values fluctuated between 600 and 865 $\mu\epsilon$. Compared to the shaded region in the partially exposed case, these strain values are higher. This difference is because of the more uniform temperature distribution under full shading, whereas sharp spatial temperature gradients in the partially exposed case produce localized changes in strain.

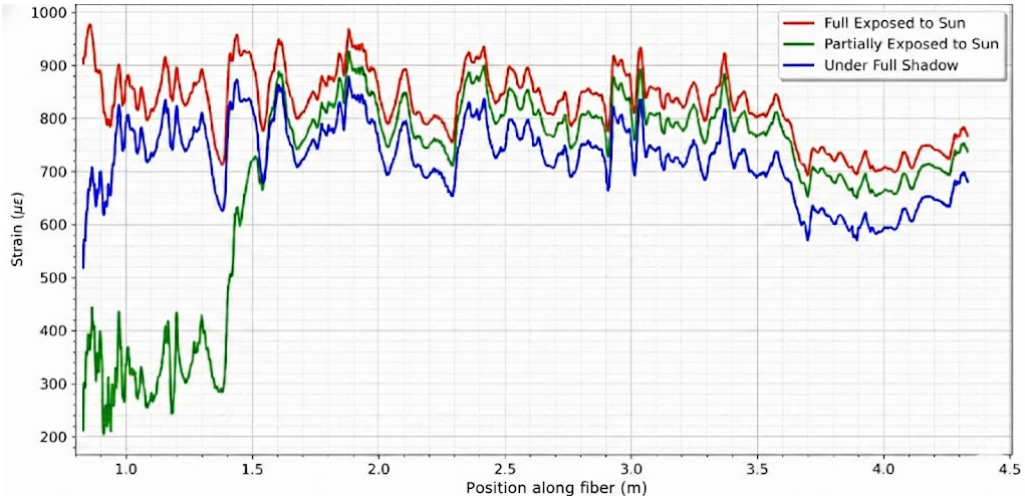

Figure 6: Bottom-surface strain variations under all scenarios

3.2.2 Top Strain

Top strain values were collected for all three exposure scenarios to evaluate the effect of high temperature on the strain response of the metal roof. The red curve in Fig. 7 represents the condition of maximum thermal expansion, in which the top surface of the roof is uniformly heated due to direct solar exposure. Under this condition, strain values remain consistently high, fluctuating between 500 and 580 $\mu\epsilon$, indicating that the material is in tension along the length of the sensor. A distinct peak is observed around the 2.6-m location, where the strain increased to 680.7 $\mu\epsilon$. This

peak corresponds to the mid span of the roof panel, consistent with the simply supported boundary condition and the location of maximum flexural deformation.

The green curve in Fig. 7 represents the partially exposed condition and shows a reversal in strain associated with the transition from shaded to sunlit regions. In the shaded section, between 0.8 m and 1.3 m, the measured strain is negative (-100.2 $\mu\epsilon$), indicating that the top surface of the panel is in compression. As the sensor passes the boundary from shade into direct sunlight, between 1.3 m and 1.6 m, the strain increases sharply and transitions to tensile values of 500.4 $\mu\epsilon$.

The blue curve in Fig. 7 represents the strain profile when the roof is under full shadow. Under this condition, the strain values are relatively stable, ranging between 400 and 500 $\mu\epsilon$. These values are significantly higher than those observed in the shaded portion of the partially exposed case (green curve), where compressive strain was measured. Overall, when the metal roof was fully exposed to sunlight, the roof temperature increases, leading to thermal expansion and placing the roof panel predominantly in tension.

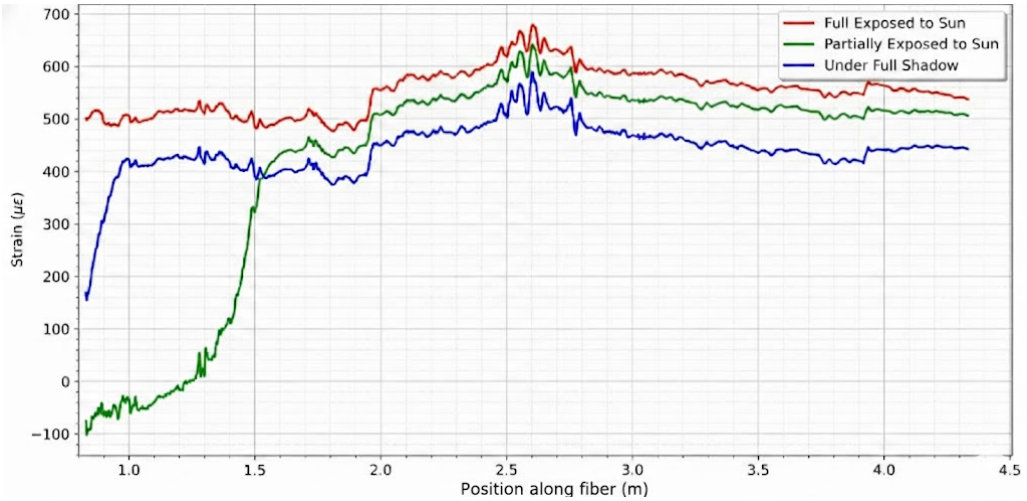

Figure 7: Top-surface strain variations under all scenarios

3.3 Wavelength

This section presents the thermal wavelengths for three environmental exposure scenarios of the metal roof: full sun exposure, partial exposure, and full shadow. Wavelength is defined as the distance between consecutive local minima. The results are summarized in Table 1 and discussed below.

For the full sun exposure case, the bottom strain profile shown in Fig. 8 was used to calculate the thermal wavelength. Under this condition, the surface temperature measured by the fiber optic sensor reaches its maximum value, resulting in significant expansion of the roof panel. The identified local minima are marked by distinct points along the bottom strain (blue), top strain (green), and temperature (red) curves. Due to the high-amplitude spatial fluctuations in this scenario, the analysis yields the longest wavelengths observed in this study, with average values of 0.310 m for bottom strain, 0.285 m for top strain, and 0.275 m for temperature. Differences in the average wavelengths represents the effect of temperature on the varying behavior of the PBR panel. While,

Table 1: Average wavelength comparison

Scenario	Bottom Strain (m)	Top Strain (m)	Temperature (m)
Exposed to Full SunLight	0.310	0.285	0.275
Partially Exposed to Sunlight	0.245	0.224	0.215
Under Full Shadow	0.170	0.155	0.145

consistent wavelength values across the temperature and strain profiles indicate a highly correlated thermomechanical response. The deformation is governed by the thermal gradient.

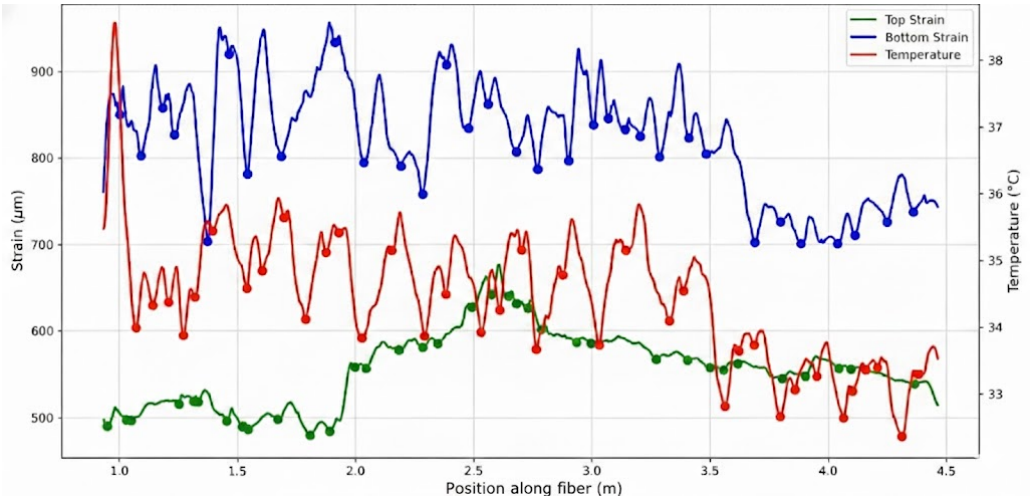

Figure 8: Temperature and strain variations, with peaks indicating wavelengths under full sunlight exposure

Bottom peaks for the partially exposed roof condition are shown in Fig. 9. As the surface temperature increases rapidly from 10°C to 30°C, the data are divided into two distinct regions: a shaded region with relatively smaller values and a sunlit region with higher values. Compared to the full sun exposure case, these results show a reduction in cycle length. The average wavelength of the bottom strain is 0.245 m, the average wavelength of the top strain is 0.224 m, and the average wavelength of the temperature is 0.215 m. The reduction in wavelength at the transition from shadow to sunlight is governed by the thermal gradient, which plays a significant role in defining the thermomechanical behavior of PBR panel.

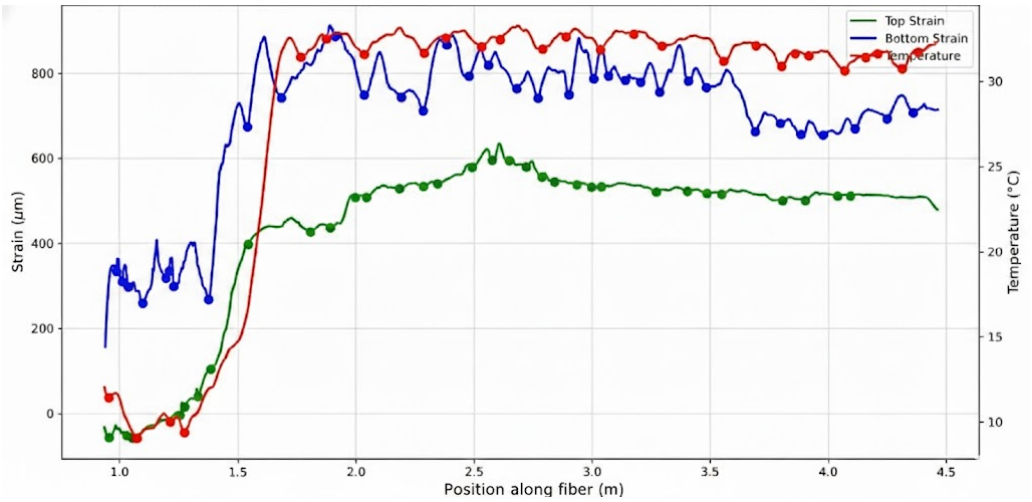

Figure 9: Temperature and strain variations, with peaks indicating wavelengths under partial sunlight exposure

Fig. 10 illustrates the wavelength characterization for the fully shaded roof condition. Despite the absence of direct solar radiation, a series of local minima was observed along the clear span of the roof. Under full shadow, the wavelengths are significantly reduced. The average wavelength of the bottom strain decrease to 0.170 m, while the average wavelengths for top strain and temperature decrease to 0.155 m and 0.145 m, respectively. These results confirm that solar exposure plays a major role in governing the thermal-mechanical response of metal roof panels.

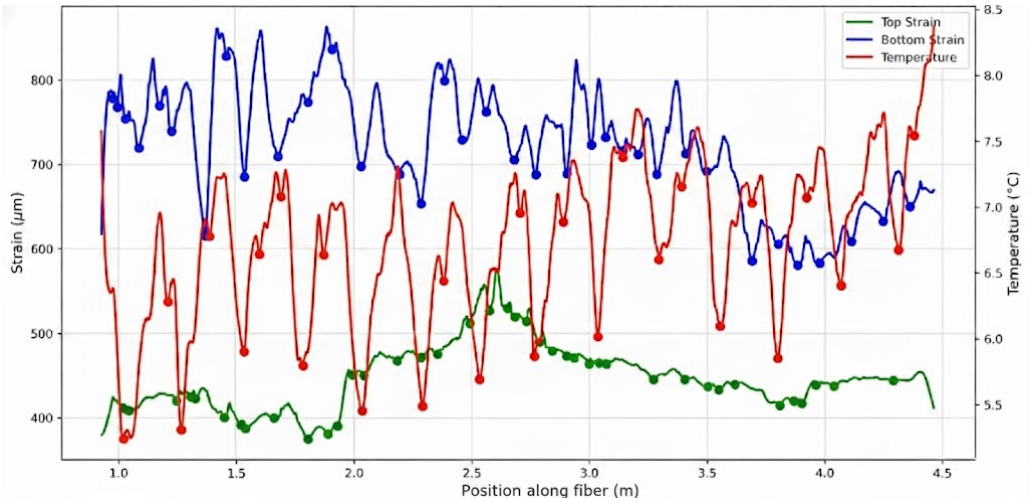

Figure 10: Temperature and strain variations, with peaks indicating wavelengths under full shadow

4 Discussion

This study investigated the thermomechanical behavior of a PBR roof panel subjected to high temperatures using distributed fiber optic sensors. By simultaneously measuring temperature and strain at high spatial resolution, the experiment captured localized strain variations and wavelength shifts along the length of the panel. The following discussion focuses on how nonuniform temperature fields drive strain development in roof panels.

A temperature gradient of 20.3°C at the shadow boundary produced localized strain concentrations. Because the shaded and sunlit portions of the roof panel experienced different thermal expansion rates, high-frequency deformation developed in the transition zone. This behavior confirms that the temperature field along the panel is nonuniform rather than producing uniform thermal expansion. The observed change in wavelength further indicates the deformation in dependent on the thermal gradient.

Comparison of the top and bottom strain sensor measurements showed that the bottom strain sensors consistently recorded higher strain values. This occurs because the bottom surface experiences two effects: bending-induced tension from dead load (self weight) and axial tension due to thermal expansion. In contrast, the top surface experiences compression from dead load and tension from thermal expansion, resulting in lower net strain values.

Solar exposure was another important factor that contributes to the nonuniform temperature field. When the roof panel was fully exposed to sunlight, all three sensors recorded their maximum values, whereas under full shading, all sensors recorded lower values. These results indicate that solar radiation plays a significant role in controlling temperature distribution along the roof span. A similar pattern was observed for the top stain and temperature sensors, while the bottom strain sensor showed different behavior due to panel deflection caused by dead load.

When roof temperature was compared with ambient air temperature on the same day, the roof temperature was 9.6°C higher. Current roof design practices typically rely on ambient air temperature; however, these results demonstrate that actual roof temperatures vary significantly throughout the day and can substantially exceed ambient conditions. The initial temperature peak observed in the measurements further highlights the influence of surrounding environmental effects, such as reflected solar radiation. This finding suggests that local thermal conditions should be considered when evaluating roof performance under extreme heat.

Future work will vary experimental parameters, including roof panel profiles, clear spans, and solar orientations. While the present study examined a single PBR panel, future research work will extend to full roof systems composed of multiple PBR panels with fasteners. Long-term monitoring will be conducted to assess cumulative thermal cycling effects over multiple seasons. These data will support the development of fatigue life prediction models that account for increasing high temperature events.

5 Conclusion

This study evaluated the thermal behavior of a metal roof panel under high temperature. Temperature and strain were monitored throughout the day under different solar exposure scenarios. The results showed that roof panels exposed to direct sunlight developed significantly higher strain than those under shaded conditions, and roof temperatures consistently exceeded ambient air temperature. A key contribution of this work is the characterization of distributed temperature and strain behavior along the full span using fiber optic sensing. The findings indicate that design based solely on ambient air temperature may underestimate actual thermal demand on roof panels.

The study also demonstrated that thermal wavelength is not constant but depends on environmen-

tal conditions, particularly surface temperature and solar exposure. This study focused on a single roof type and support condition and therefore requires further testing under different configurations and conditions. Although the present study focused on a single roof profile and support condition, the results provide important insight into the effects of high diurnal temperatures which may concerns increasing heatwave intensity on metal roofs. Additional testing under varied configurations is required before generalization. Despite these limitations, this work contributes to improved understanding of the thermal–mechanical response of metal roof panels under high heat conditions.

Acknowledgment
The authors sincerely thank ASC Profiles for providing the PBR roof panels used in this experimental study. This support was essential to the research and is greatly appreciated.

References

Chong, C., Wang, M., Liu, D., Lu, Y., Cai, W., Song, D., and Liu, X. 2025. "Assessing the Effects of Long-Term Temperature Fields on the Performance of a Metal Roof System with Measured Temperature Field Distributions". *Journal of Constructional Steel Research*, 228 p. 109427.

Dabral, A. and Ewing, B. T. "Analysis of Wind-Induced Economic Losses Resulting from Roof Damage to a Metal Building". *Journal of Business Valuation and Economic Loss Analysis*.

Liu, Z., Ji, C., Shi, G., and Mo, Y. 2025. "Structural Safety Risk Prediction Method for Terminal Building Steel Roof Construction Considering Spatial and Temporal Variations". *Journal of Constructional Steel Research*, 224 p. 109126.

Lu, P., Lalam, N., Badar, M., Liu, B., Chorpening, B. T., Buric, M. P., and Ohodnicki, P. R. 2019. "Distributed Optical Fiber Sensing: Review and Perspective". *Applied Physics Reviews*, 6 (4) p. 041302.

Ma, S., Xu, Y., Pang, Y., Zhao, X., Li, Y., Qin, Z., Liu, Z., Lu, P., and Bao, X. 2022. "Optical Fiber Sensors for High-Temperature Monitoring: A Review". *Sensors*, 22 (15) p. 5722.

Roman, M., Balogun, D., Zhuang, Y., Gerald, R. E., Bartlett, L., O'Malley, R. J., and Huang, J. 2020. "A Spatially Distributed Fiber-Optic Temperature Sensor for Applications in the Steel Industry". *Sensors*, 20 (14) p. 3900.

Viljoen, E. and Hugo, J. 2024. "The Efficacy of Roof-Based Adaptations to Reduce Heat Stress Exposure in Informal Dwellings". *Acta Structilia*, 31 (2) pp. 42–80.

Wang, D., Xin, Z., Wang, M., Ou, T., Mao, J., Zhu, Y., and Tan, J. 2022. "Analysis of Temperature Field and Effect of Cold-Formed Stainless Steel Roof Panels". *Journal of Constructional Steel Research*, 198 p. 107575.

Wang, J.-T., Liu, Y.-F., Zhou, M., Nie, J.-G., and Chen, X. 2023. "Deformation Prediction of Large-Span Spatial Structure Considering Adverse Weather Conditions". *Structures*, 50 pp. 508–523.

Wang, M., Liu, D., Lu, Y., Yang, Q., Song, D., and Liu, X. 2025. "Investigation into the Nonuniform Temperature Effect of a Large-Span Stainless Steel Roof System under Solar Radiation". *Journal of Constructional Steel Research*, 224 p. 109133.

Wang, M., Xin, Z., Ou, T., Wang, D., and Zhang, Y. 2023. "Experimental Study on Temperature Field and Effect of Standing Seam Stainless Steel Roof System with Different Structures Forms". *Structures*, 49 pp. 198–211.

Xu, W., Chen, D., and Qian, H. 2020. “Non-Uniform Temperature Fields and Effects of Steel Structures: Review and Outlook”. *Applied Sciences*, 10 (15) p. 5255.

Yang, S., Homa, D., Heyl, H., Theis, L., Beach, J., Dudding, B., Acord, G., Taylor, D., Pickrell, G., and Wang, A. 2019. “Application of Sapphire-Fiber-Bragg-Grating-Based Multi-Point Temperature Sensor in Boilers at a Commercial Power Plant”. *Sensors*, 19 (14) p. 3211.

Zhou, M., Fan, J.-S., Liu, Y.-F., Zhang, J.-X., Duan, X.-J., and Lei, S.-S. 2020. “Non-Uniform Temperature Field and Effect on Construction of Large-Span Steel Structures”. *Automation in Construction*, 119 p. 103339.